Monthly Notices
of the
ROYAL ASTRONOMICAL SOCIETY

Mon. Not. R. Astron. Soc. **406,** 237–246 (2010) doi:10.1111/j.1365-2966.2010.16703.x

Subpulse modulation, moding and nulling of the five-component pulsar B1737+13

Megan M. Force[1⋆] and Joanna M. Rankin[1,2⋆]

[1]*Physics Department, University of Vermont, Burlington, VT 05405, USA*
[2]*Sterrenkundig Instituut 'Anton Pannekoek', University of Amsterdam, NL-1090 GE Amsterdam, the Netherlands*

Accepted 2010 March 15. Received 2010 March 15; in original form 2009 June 23

ABSTRACT

Recent Arecibo polarimetric observations of the bright five-component pulsar B1737+13 have facilitated a comprehensive new analysis of its pulse-sequence modulation phenomena. The bright leading component in the star's profile, as well as its other conal components, exhibit a roughly periodic, longitude-stationary modulation with an effective P_3 of about nine rotation periods. We also find that they show a much slower periodicity at ∼92 rotation periods. Correlation analyses reiterate these regularities and suggest a modulation pattern moving through the profile negatively. These various properties are largely compatible with a rotating subbeam-carousel model having typically 10 'beamlets'. Polar maps are given showing typical subbeam structures that are compatible with the pulsar's somewhat unstable modulation. Geometric analysis finds the central component lagging the centre of the traverse of the polarization position angle, suggesting possible effects of retardation and aberration. There remains little overt evidence for the two modes identified previously. Unlike B1237+25, this pulsar exhibits few if any true nulls, and its core emission is relatively steady.

Key words: pulsars: general – pulsars: individual (B1737+13).

1 INTRODUCTION

The average pulse profile has often been regarded as the 'signature' of a particular pulsar and an important source of information about its emission geometry. While fewer than a dozen pulsars are known to exhibit five distinct profile components, this group is significant because they display the full complexity of core/cone emission. As is well known (e.g. Rankin 1993a,b, hereafter ET VI), a pulse profile with five components is thought to represent a sightline traverse through two concentric cones and a core beam (see Fig. 1). Observations of these stars generally reveal a nearly central sightline traverse of the polarization position angle (hereafter PPA). The hollow emission cones are thought to consist of 'carousel' subbeam systems rotating about a star's magnetic axis. The progressive broadening of profiles with wavelength supports this conclusion (e.g. Mitra & Rankin 2002), as does the demonstration of carousel action in a number of pulsars [e.g. B0943+10 (Deshpande & Rankin 2001, hereafter DR01); B0834+06 (Rankin & Wright 2007) and J1819+1305 (Rankin & Wright 2008)]. These and other recent papers have established multiple connections between the 'big three' pulsar modulation phenomena, drifting subpulses, moding and nulling (e.g. Herfindal & Rankin 2007, 2009, hereafter HR0709).

Recent single-pulse studies of three five-component pulsars, B1237+25, B1857−26 and B0329+54, have provided intriguing new insights into their moding, nulling, subbeam-carousel and core-emission characteristics. In a detailed analysis of several pulse sequences (hereafter PSs) of B1857−26, Mitra & Rankin (2008) found evidence for a subbeam carousel of 20 beamlets, using the methods described in DR01. In a 2005 study of PSs of the best known core/double-cone pulsar, B1237+25 (Srostlik & Rankin 2005, hereafter SR05) found a previously unknown emission behaviour, intermediate between the pulsar's well-known normal and abnormal modes (Backer 1970), and Maan & Deshpande (2008) found a likely tertiary period. Further, that (i) 'nulls' in many pulsars show slow, amplitude-modulated periodicities (HR0709) – that is, fluctuation-spectral 'features' – and such short *pseudo*-nulls appear to result from 'empty' sightline traverses through 'carousel' subbeam systems, (ii) periodicities are seen in a large proportion of all pulsars (Weltevrede, Edwards & Stappers 2006; Weltevrede, Stappers & Edwards 2007) and (iii) mode-changing and nulling are closely connected (Wang, Manchester & Johnston 2007) raise further intriguing questions about double-cone pulsars. Finally, Mitra et al.'s (2007) investigation of pulsar B0329+54's polarized core emission has revealed intensity-dependent aberration/retardation (hereafter A/R) effects apparently reflecting the primary acceleration or amplification process in this star.

These recent results prompted our renewed interest in pulsar B1737+13 – the second brightest member of the core/double-cone species within the Arecibo sky – which had received no detailed study in many years. Hankins & Rickett (1986) first clearly

⋆E-mail: megan.force@uvm.edu (MMF); joanna.rankin@uvm.edu (JMR)

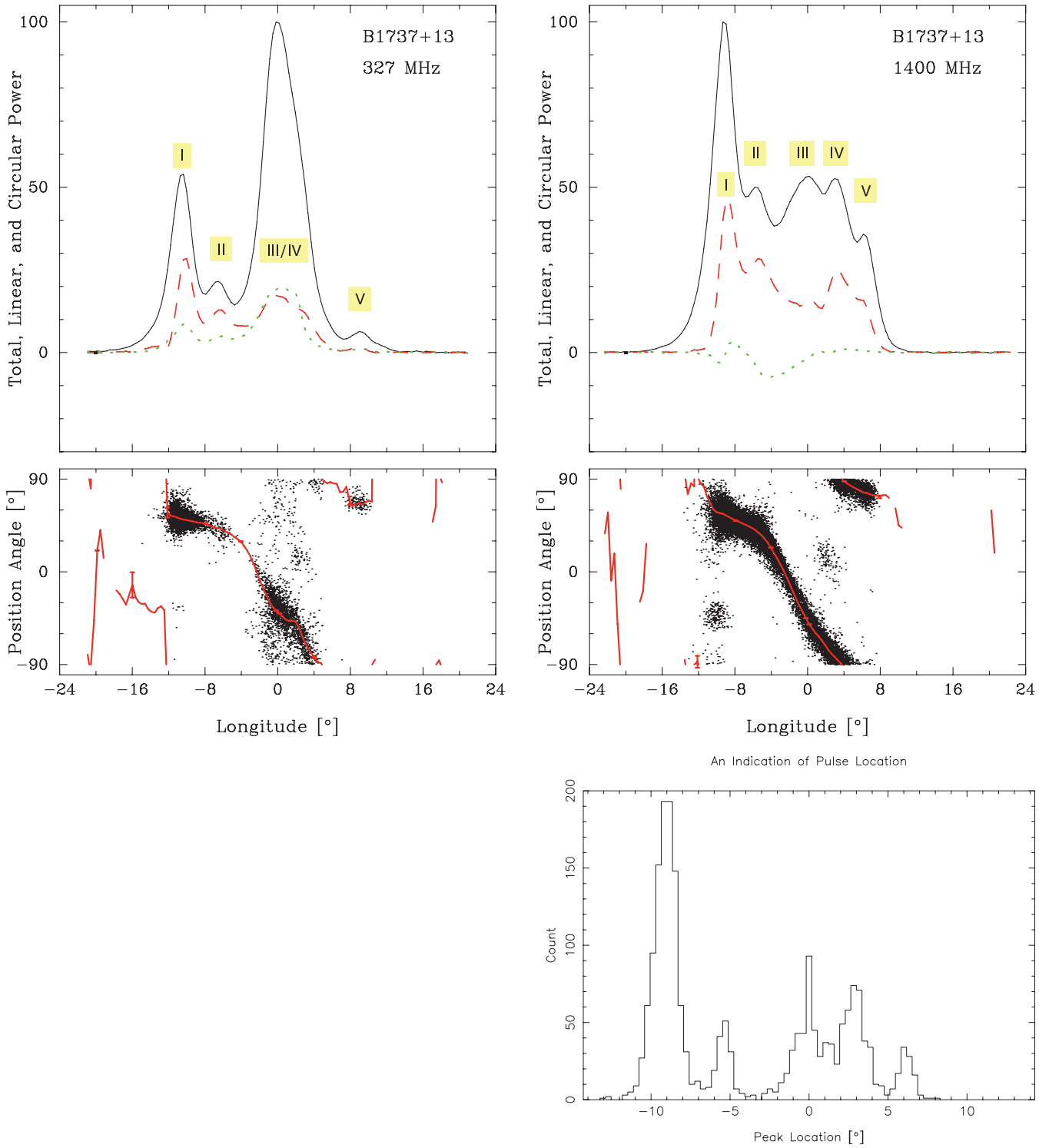

Figure 1. Polarization position angle (PPA) histograms for B1737+13 at 327 MHz (upper left-hand panel) and 1400 MHz (upper right-hand panel) comprising 2241 and 2055 pulses, respectively. The two panels display the total power (Stokes I), total linear polarization [L ($= \sqrt{Q^2 + U^2}$); dashed red], circular polarization (dotted green) (upper) and the polarization angle PPA[$= (1/2)\tan^{-1}(U/Q)$] (lower). Individual samples that exceed an appropriate $>2\sigma$ threshold appear as dots with the average PPA (red curve) overplotted. The PPAs are approximately absolute (see text). The tiny rectangle at the left-hand side of each upper panel gives the resolution and a deflection corresponding to three off-pulse noise standard deviations. The histogram of peak pulse intensity (lower right-hand panel) at 1400 MHz corresponds to the profile in the upper right-hand panel. The star's five components are clearly discernible at this frequency, although at metre wavelengths components III and IV become conflated or even merged as in the 327-MHz profile.

delineated the star's five components, distinguishing its components III and IV through their distinct spectra. Deich (1986) discovered the star's roughly 10 rotation period modulation, seen primarily in component I. Early profile polarization measurements (Rankin, Stinebring & Weisberg 1989) confirmed the expected steep PPA traverse and sense-reversing circular polarization associated with the central component III. More recent profile polarimetry over a broad-band (Gould & Lyne 1998; Hankins & Rankin 2010) clearly shows that the core component exhibits a steeper spectrum as usual, evolving from relative weakness at high frequencies to dominate the profile at long wavelengths.

The most thorough published study of B1737+13 was carried out more than 20 yr ago (Rankin, Wolszczan & Stinebring 1988, hereafter RWS), but in current terms now leaves most questions unaddressed. Based on 1400-MHz observations, the paper argues that the star exhibits two distinct modes: one with bright, roughly periodic, longitude-stationary (11–14 P_1) emission in component I and the other without it. They found no discernible periodic modulation associated with components II–IV, but their quasi-2D cross-correlation function (CCF) identified a strong correlation between components I and V and between components II, III and IV.

In this paper we revisit this pulsar using the new methods of investigation employed in DR01 and SR05. In Section 2 we discuss our observations, and in Section 3 the geometry of the pulsar's emission. Section 4 is dedicated to analysis of the core component, and in Section 5 we treat the PSs of B1737+13, including nulling and moding phenomena and the observed low-frequency feature. In Section 6 we summarize our results.

2 OBSERVATIONS

The observations were carried out using the 305-m Arecibo Telescope in Puerto Rico. They used the upgraded instrument with its Gregorian feed system, 327 MHz (*P* band) or 1100–1600 MHz (*L* band) receiver, and Wideband Arecibo Pulsar Processor as described in Rankin & Wright (2008). The March 2008 observation has three bands combined to give 300-MHz bandwidth. The interstellar and ionospheric contributions to the rotation measure were separately determined for each observation (Rankin & Weisberg, in preparation), and these values used to rotate the PPAs to infinite frequency; therefore the PPAs are approximately absolute. The date, resolution and the length of the observations are listed in Table 1.

Table 1. Observational parameters.

Frequency (MHz)	Bandwidth (MHz)	Date (m/d/yr)	$\Delta\varphi$ (°)	Length (pulses)
1400	300	03/12/08	0.11	2055
1425	100	04/10/03	0.23	1022
327	25	01/06/05	0.23	2241

3 GEOMETRY

Fig. 1 displays the five-component average profile of B1737+13 at 327 and 1400 MHz. At the lower frequency, the central (putative core) component dominates the profile and appears to merge with component IV. In both cases we see a steep traverse of the PPA near the centre of the profile representing around -20° deg^{-1}. As the PPAs are approximately absolute, the two PPA traverses roughly track each other, and one can see that several of the Orthogonal Polarization Mode (OPM) 'patches' in the two profiles correspond.[1] The geometric analysis in ET VI used this value and the profile dimensions to estimate the magnetic latitude angle α and sightline impact angle β as 41° and 1°.9 – such that β/ρ (where ρ is the outside half-power point of the beam) is 0.40 and 0.28 for the inner and outer cones, respectively. The polarization information provides no clear indication of the sign of β – i.e. whether the sightline traverse is poleward or equatorward of the magnetic axis. The above analysis demonstrates that the conal beam dimensions of B1737+13 are very nearly identical to those of many other pulsars as scaled to the angular size of the polar-cap emission zone. Lyne & Manchester's (1988) method of geometric analysis results in just the same α and β values if their less steep PPA value is corrected.

Also intriguing are the separations of the conal component pairs in relation to the various possible markers of the profile centre. Both profiles are asymmetric in that the core lags the mid-points of both conal pairs, a situation that is possibly indicative of A/R (e.g. see Malov & Suleymanova 1998; Gangadhara & Gupta 2001, hereafter G&G). We can then use G&G's method (as corrected by Dyks, Rudak & Harding 2004) to estimate the emission heights of the conal emission in relation to that of the core. The analysis is then virtually identical to that carried out for B1237+25 in SR05, Table 1, except that here we have little option but to take the peak of the core component as marking the longitude of the magnetic axis. Values are then given in Table 2 corresponding to the asymmetric separations of the leading and trailing components with respect to the core component. At 1400 MHz, the measurements are based on both the profile and peak-occurrence histogram in Fig. 1. At 327 MHz only the profile was available, and the merged components III and IV make estimation of the latter's position difficult; however, careful inspection shows an inflection on the trailing side of the feature which gives good guidance.

[1] Interestingly, Hobbs et al.'s (2005) determination of B1737+13's proper-motion direction of $227^\circ \pm 6^\circ$ gives the possibility that the fiducial PPA is aligned with the star's velocity vector in the sense of Johnston et al. (2006) and Rankin (2007). The value given by Johnston et al. for B1737+13's fiducial PPA is $-46^\circ \pm 4^\circ$ – which is in good agreement with the PPAs at the profile centres in Fig. 1 – making its orientation relative to the star's rotation axis around $87^\circ \pm 7^\circ$. If, following Mitra, Rankin & Gupta (2007), we could assume that the pulsar's rotation and velocity vectors are aligned, then we should associate its primary polarization mode with the extraordinary (X) propagation mode.

Table 2. Aberration/retardation analysis results for B1737+13.

Frequency/cone	ϕ_l^i (°)	ϕ_t^i (°)	ν^i (°)	Γ^i (°)	$r^i{}_{\rm em}$ (km)	s_L^i
1400/II	-9.10 ± 0.10	6.19 ± 0.10	-1.46 ± 0.07	5.45 ± 0.06	487 ± 24	0.56 ± 0.01
327/II	-11.50 ± 0.25	8.50 ± 0.25	-1.50 ± 0.18	6.94 ± 0.16	502 ± 59	0.71 ± 0.04
115.5/II	-13.30 ± 0.50	10.50 ± 0.50	-1.40 ± 0.35	8.17 ± 0.32	468 ± 118	0.86 ± 0.11
1400/I	-5.52 ± 0.20	2.85 ± 0.20	-1.34 ± 0.14	3.38 ± 0.11	447 ± 47	0.36 ± 0.02
327/I	-6.79 ± 0.30	3.50 ± 0.40	-1.65 ± 0.25	3.93 ± 0.21	550 ± 84	0.38 ± 0.03

The results in Table 2 are generally compatible with other pulsars with double-conal emission. The (2σ) estimation errors are significant for all of the values and indicate emission heights of roughly 500 km, just over twice those estimated using the last-open-field-line geometry (e.g. in ET VI). Also, the inner cone emission appears to reflect a more interior annulus of field lines on the polar cap than that of the outer cone. Interestingly, the core appears to lag behind the steepest gradient (or centre) point of the PPA traverse in both the 327- and 1400-MHz profiles of Fig. 1 (although this point is not easy to fix with any accuracy).

4 CORE COMPONENT

Given the rich and intriguing effects associated with the core emission in such pulsars as B0329+54 (Edwards & Stappers 2004; Mitra et al. 2007) and B1237+25 (e.g. SR05), we have examined the behaviour of B1737+13's core component carefully. Unfortunately, however, our efforts have given little return. We identify this 'core' mainly by virtue of its position in the centre of the profile (i.e. component III); it does show a steeper spectrum than the conal components, but it is hardly marked by antisymmetric Stokes *V* at 1400 MHz and not at all in the 327-MHz observation. In both observations the core component exhibits evidence of OPM-produced linear depolarization, and a small population of secondary polarization-mode samples can be discerned on the leading and trailing edges of the core feature.

We have also studied the core emission dynamically, but as can be seen in the colour-intensity displays of Fig. 2, its intensity varies over a narrow range and often it is difficult to distinguish from component IV. In both the 327- and 1400-MHz PSs, we find that the core participates weakly in the low-frequency modulation seen more prominently in the conal components (see below). Longitude–longitude CCFs at zero delay (not shown) do confirm that the core fluctuations are largely independent of component IV, and others at delays of a few periods show little significant correlation with the other components.

5 PULSE-SEQUENCE ANALYSES

5.1 'Modes' and modulation

In their 1988 paper, RWS discussed B1737+13's emission properties in terms of two modes, 'normal' and 'abnormal', which differed primarily in the relative strength of component I (see their fig. 4). Using an early form of cross-correlation analysis, they found the somewhat unstable normal mode to be characterized by an approximately periodic strengthening of the first component on a cycle of approximately 11–14P_1. They then identified PS intervals lacking bright (or periodic) component I emission as representing an abnormal mode. A typical 400-P_1 PS similar to those RWS studied is shown in Fig. 2 on two different intensity scales (both coded as in Fig. 3 – that is, blue up through green to red and saturating in magenta): one (left-hand side) displays the low-intensity emission; whereas the other (right-hand side) depicts even the most intense subpulses such that most do not saturate in magenta. While some regularity is discernible, only in the interval between pulses 650 and 750 do we see the bright $\sim$10P_1, component I modulation characteristic of RWS's 'normal mode'. We do see that the rough periodicities are not confined to component I, but often modulate components II–IV as well. The modulation appears stationary, with no apparent subpulse motion or drift. Bright component V subpulses do seem to accompany bright component I emission as reported by

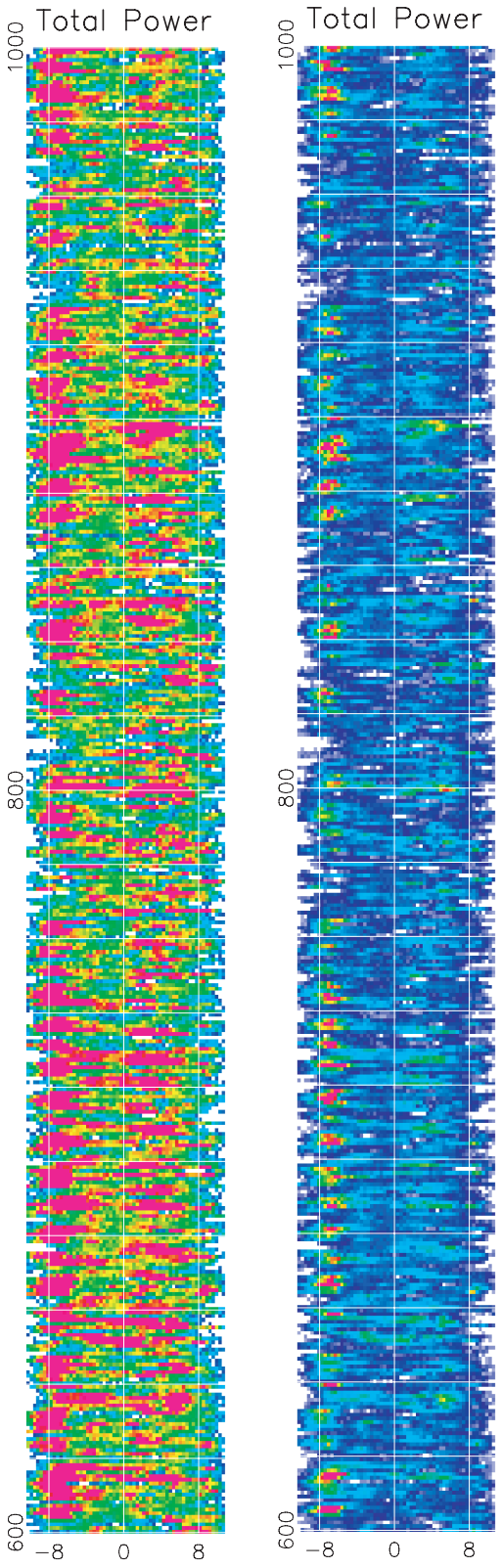

Figure 2. Stokes *I* is shown for a 400-pulse, 1400-MHz PS using a saturated low-intensity (left-hand image) and little saturated high-intensity (right-hand image) scale (as in the Fig. 3 colour bar). Rough periodicity in component I is apparent, as is the so-called 'abnormal' mode, which lacks strong emission here (see text). The origin here is shifted relative to Fig. 1 so that the cones are symmetric about zero longitude [causing the core (comp. III) to lag].

RWS, but we will see below that this correlation is not very strong. Finally, note that this putative interval of RWS's 'normal mode' shows no clear boundaries.

Fig. 3 gives longitude-resolved fluctuation (LRF) spectra for the 1400-MHz observation, and a rough, broad feature peaking at around 0.10–0.11 cycles period^{-1} (hereafter c/P_1) corresponds to the normal-mode modulation discussed by RWS. A harmonic resolved fluctuation spectrum (not shown) displays a nearly symmetrical integral spectrum, indicating primarily amplitude (as opposed to phase) modulation – as would be expected for this star's geometry, wherein the sightline traverses the emission cones radially. The LRF spectra of short intervals of the PSs show either a broad response or discrete features with P_3 values in a similar range between around 8 and 10P_1.

Our further analysis suggests that the prominence of component I varies broadly in different sections of our PSs. On closer inspection we were unable to identify any reliable criterion for assigning specific pulses (or short trains of pulses) to one or the other of RWS's putative modes – a situation very unlike that for other pulsars with several modes. Using fluctuation-spectral methods, we find that intervals of weak component I emission continue to show its characteristic rough periodicities, although at a weaker level of intensity and with less clearly correlated emission in the other components. Conversely, when component I is active, correlated emission is often seen in components III–V, suggesting some tendency to periodicity in the core as well as both cones. Therefore we find little cause to regard RWS's modes as similar to the discrete changes of mode seen in other stars (e.g. B1237+25). We will thus continue to use their terms below as descriptors, but without implying the mode-changing phenomenon.

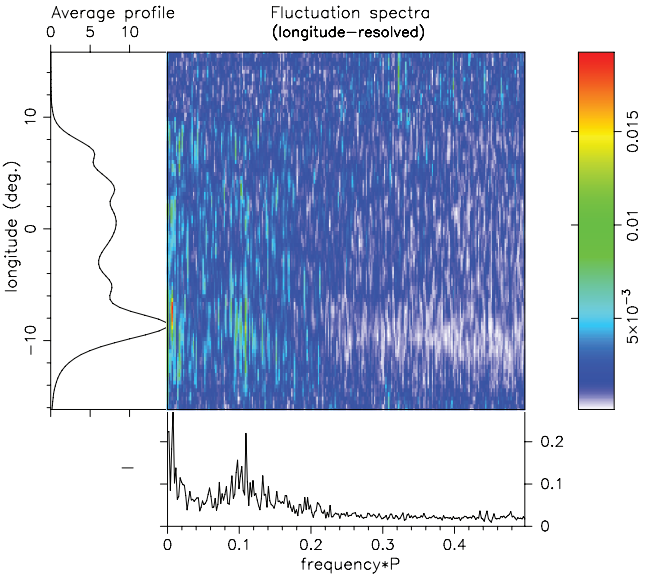

Figure 3. Longitude-resolved fluctuation spectra for the entire B1737+13 PS at 1400 MHz, employing an FFT length of 512. The spectra (main panel) are shown relative to the average profile (left-hand panel) and colour-intensity coded according to the right-hand bar, with the integral spectrum given in the bottom panel. The colour scale is in arbitrary units of flux density. The broad 'hump' of fluctuation power peaking at 8–10P_1 surely represents RWS's normal-mode modulation. In specific intervals the star's emission is modulated at frequencies some 0.11 c/P_1, corresponding mainly to periodicities of around 9.1 ± 1P_1. The surprisingly narrow low-frequency feature, however, was not identified by RWS, and we will consider its significance further below.

5.2 Low-frequency and 'drift' modulation features

The existence of a low-frequency modulation feature is shown in Figs 3 and 4. The feature may also be discerned in the component I panel of the 92-cm 2D fluctuation spectra of Weltevrede et al. (2007). Our long PSs were analysed in an effort to determine the frequency of this feature as precisely as possible. Values were encountered between 80 and 120P_1 in sections of 256 pulses, reflecting the large estimation errors. A value of 91P_1 with a 2σ error of ±2P_1 was determined for our 1400-MHz PS using a fast Fourier transform (FFT) of length 2048 (see Fig. A1). This low-frequency fluctuation is also predominantly amplitude modulation as shown by its symmetrical harmonic resolved fluctuation (HRF) spectra (not shown).

The 327-MHz PS LRF (see Fig. A2) is similar to that above in that it shows a strong, narrow 'drift'-modulation feature reflecting a periodicity of around 8.98 ± 0.10P_1, but different in that we see no bright low-frequency feature. In order to assess the effect and persistence of this modulation, we tried shorter LRFs and found that the above modulation is stable only over a central region of the PS (pulses 400–2000). We then folded this central interval at the roughly 90P_1 period of the low-frequency feature above – here 10 times the above or 89.8P_1, and the result is shown in Fig. 4 with the non-fluctuating power ('base') removed. Note, for instance, that the amplitude of component I fluctuates over a range from blue to red in the main panel (up to 35 units of relative intensity) in addition to a base amplitude of roughly 25 units, so the modulation is strong and regular enough to be 60 per cent modulated over the 1600-pulse interval. Components II–IV also show fluctuations at this period, and there is a hint that component V does as well.

The correlation plots in Fig. 5 explore the significance of this long periodicity using the 2055-pulse 1400-MHz observations. The top panel shows that the total single-pulse correlation peaks at multiples of the roughly 9P_1 delay, but that there is also a strong secondary peak at 91 or 92P_1. The various longitude–longitude correlation plots at different delays reiterate findings, but in greater detail. We see in the bottom display that component I is not only correlated with itself, but also with component V at a delay of 92P_1, even when averaged over the entire PS. Within the subbeam-carousel model, the 9-P_1 feature represents a median value of the drift-modulation period, P_3, and the long-period modulation at 92P_1 could be associated with the carousel circulation time $\hat{P}_3$. Thus taken together, they could be indicative of a carousel having roughly 10 'beamlets' or 'sparks'.

Some further indications regarding the structure of the putative carousel are seen in Fig. 6, where similar 327-MHz correlation plots are given for delays of both one (upper) and nine (lower) rotation periods. Immediately one is struck by the cross-like form of the correlation maps. These show that at 327 MHz most of the correlation is between components II and IV. However, at a delay of one period, significant correlation is seen between component I (abscissa) and components II, IV and V (ordinate) – and note that this correlation is asymmetric in that it occurs in the upper diagonal half of the plot only. This correlation is then between the −1 pulse delayed components II, IV and V and the undelayed component I, suggesting that the carousel rotates component V around to component I. Component II, by contrast, shows a symmetrical correlation with component IV for one-period delay, suggesting that the geometry is such that carousel rotation brings these two components into the sightline together. The nine-period delay plot (bottom) also

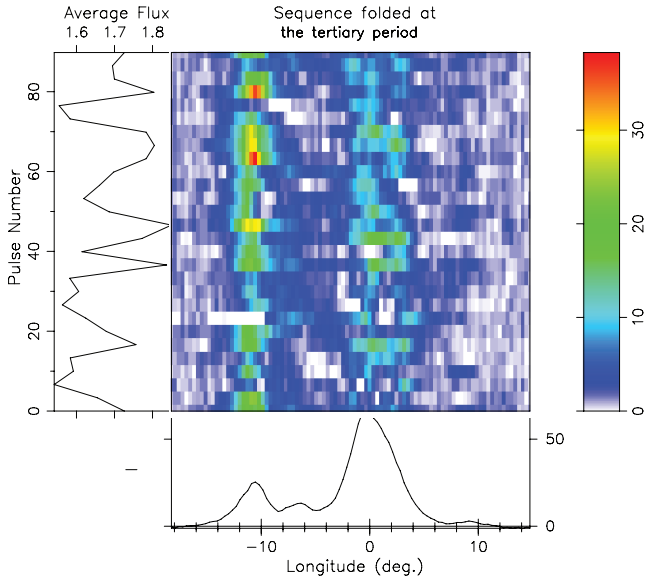

Figure 4. Display of the 327-MHz observation folded at 10 times the primary 8.98 ± 0.10P_1 modulation periodicity in this PS. Only pulses 401–2000 were used where the modulation is most stable (Fig. A2). Component I shows a large corrugation, as its peak intensity (main panel) exceeds its 'base' (unmodulated power; bottom panel) intensity. This 'base' is removed in the main panel to show this clearly. The colour scale to the right-hand side of the image gives the modulation amplitude. Components II and IV are also comparably modulated, but their modulation moves only from blue through cyan to green (note the separate component IV modulation power at about +4° longitude). Even component III shares in this modulation at the 10 per cent level; and there is a suggestion of it in component V as well.

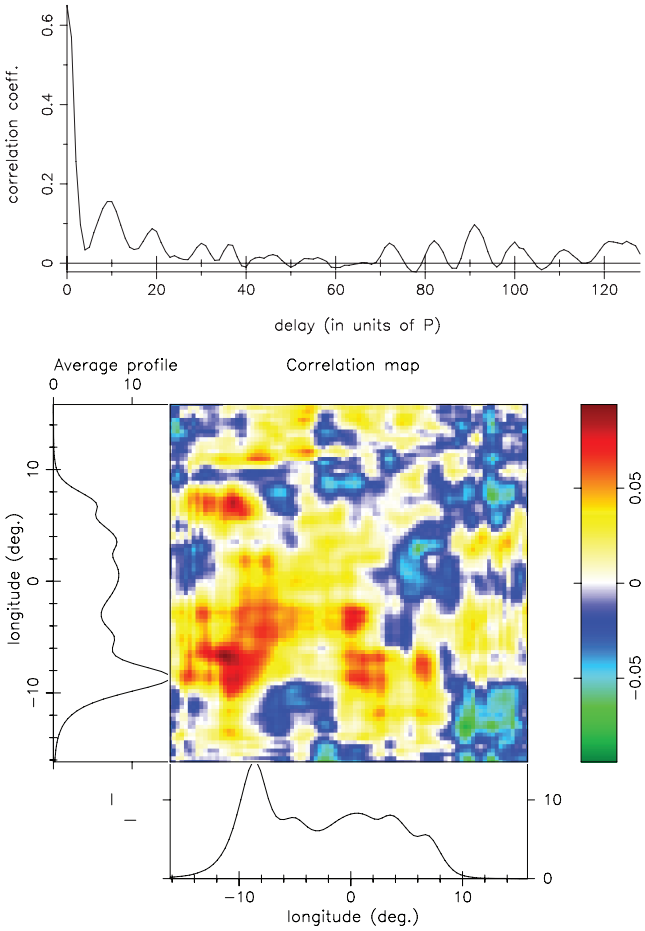

Figure 5. Correlation plots computed from the 2055-pulse, 1400-MHz PS. Top: a total (or 'diagonal') correlation plot showing how individual pulses correlate with themselves for delays up to 128P_1. Note the large peak at the 9P_1 primary modulation period as well as a significant peak at about 92P_1. The three-standard-deviation error in this correlation is about 0.4 per cent. Bottom: a longitude–longitude correlation plot showing the character of the correlation at a delay of 92 periods. Although component I shows peaks of correlation with itself at multiples of 9P_1, the 92-P_1 secondary peak is clearly significant. Note also the correlation between components I and V in the lower plot, which is expected in the rotating subbeam-carousel model. The 3σ error in this correlation map is about 6 per cent. The ordinate is delayed with respect to the abscissa, and the display shows the correlation for positive delay below the diagonal and that for the negative delay above it.

emphasizes the inner conal components II and IV which are well correlated at an interval corresponding to P_3. The weak correlation between the delayed component I and the undelayed component V also suggests that the 'beamlet' pattern rotates negatively through the profile.

5.3 Nulling

Much has been learned recently about beamlet carousel systems from the study of 'null' pulses, so we were eager to see whether B1737+13 would follow suit. In his 1981 analysis, Backus concluded that B1737+13 displayed a null fraction of less than or equal to 0.02 per cent. Of the three observations considered here, we were able to identify apparent nulls in only one, that at 1425 MHz, and then only in two instances. Both occurred during 'abnormal-mode' intervals when component I was weak or absent. A population of weak pulses, of course, occurs in all three PSs, but the weakest of these are strong enough (and the sensitivity good enough) that they can be distinguished from the baseline noise distribution. Therefore, we tend to believe that nulls do occur in the pulsar but very rarely – and two pulses in some 5000 is 0.04 per cent. Such nulls probably do not represent cessations of the pulsar's emission but are the pseudo-nulls identified in other pulsars (e.g. HR0709). Our attempts to test this by identifying periodicities in populations of nulls and weak pulses were unsuccessful.

5.4 Subbeam-carousel structure

We are now in a position to explore whether the various modulation properties identified in the foregoing sections can be produced by a rotating 'carousel' of subbeams. The 1400-MHz analyses above have provided consistent evidence for a low-frequency modulation of approximately 91P_1 that could represent its circulation time $\hat{P}_3$, and the primary subpulse modulation with a P_3 of around 8–10P_1 could be produced by subbeams passing through the sightline having an appropriate range of angular (and thus time) separations. In order to apply the techniques developed by DR01 – in particular their cartographic transformation – it is also important to know the star's basic geometry and the fiducial longitude of the magnetic axis. For the former we can depend on the analysis of ET VI (see Section 3), and for our purposes here we can estimate the latter point to lie in the very centre of the profile – that is, equidistant between the leading and trailing conal components. Referring to the measurements in Table 2, we can see that this fiducial point leads the core peak by around 1°.5. Finally, we have seen some

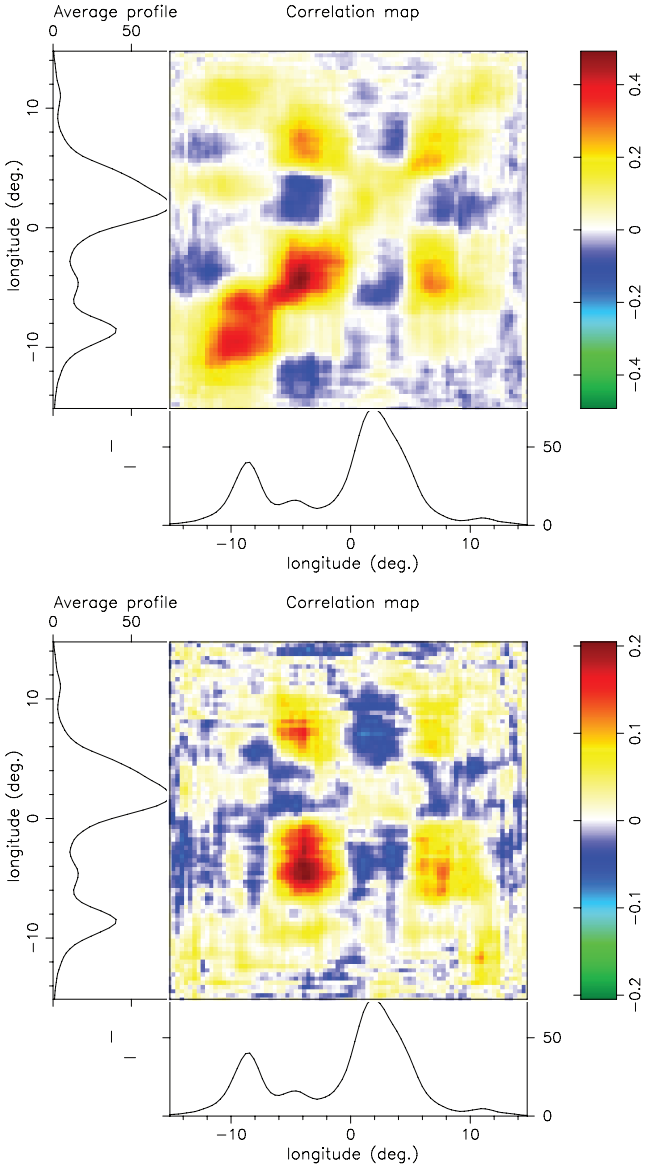

Figure 6. Correlation maps as in Fig. 5 at delays of 1 (top) and $9P_1$ (bottom) for the 327-MHz PS. The inner conal components II and IV are highly correlated, giving the diagonal 'cross' of significant correlation. Note, however, the significant and asymmetrical correlation of component I with components II, IV and V in the upper diagram at -1 period delay, which strongly suggests that the carousel rotates negatively through the emission pattern.

evidence above to the effect that the putative carousel pattern rotates negatively through the star's profile; this sense makes little difference for B1737+13 given its dominant amplitude-modulated first component and central sightline traverse. However, this information proves useful for the analysis below.

With the above necessary geometry defined, we can proceed to construct maps of the B1737+13 emission region. Given that the star's modulation is somewhat irregular, it is important to look at both short intervals showing a particular behaviour and longer sections where we may see particular behaviours persist. Starting with the latter, the second half of the 2055-length, 1400-MHz PS exhibits a strong, narrow modulation feature with a P_3 of $9.1 \pm 0.1P_1$. Fig. 7 shows this interval folded at 10 times this period, and a pattern of four component I 'beamlets' can be seen that persist in this average over around 10 circulation times. We take this corrugation as strong evidence that this folding period does represent the circulation time, and indeed adjacent values tend to exhibit patterns with less fractional amplitude.

The lower display in Fig. 8 then shows the corresponding polar map, and it is dominated by four bright 'beamlets' as expected. Note that these four 'beamlets' have magnetic azimuthal separations of about 36° ($= 360^\circ/10$), and they would thus generate a strong 'drift'-modulation feature in fluctuation spectra with a P_3 of about $9P_1$ – this largely irrespective of the remaining weak 'beamlets' in the outer cone orbit. By contrast, we have also mapped the beginning 1047 pulses in the top display of Fig. 8 in order to emphasize that this somewhat similar pattern produces no strong P_3 feature, but rather a broad 'hump' of modulation in the interval from about 0.07 to 0.12 c/P_1. This latter pattern does have some 'beamlets' with a nearly 36° spacing, but most have narrower spacing that would produce higher modulation frequencies.

The colour scale in Fig. 8 is somewhat saturated to show the inner cone region more clearly. Here the very rough pattern of inner ring 'beamlets' is 'in focus' showing that some power here also exhibits the 91-P_1 cyclicity. Recall from Fig. 6 that the inner conal components II and IV exhibited strong correlation at a delay of $9P_1$, which is far more than that did by the outer pair. We see evidence here that the 'beamlets' in the two cones exhibit a kind of 'lock–step' relationship that could explain their similar modulation patterns and mutual correlations.

Finally, we created a series of polar maps using overlapping sections of the 327- and 1400-MHz observations, which can be viewed online as 'movies' (see http://www.uvm.edu/∼jmrankin under 'Research' and 'Images and Movies'). Each frame shows the carousel 'beamlet' pattern for a single circulation time of around $92P_1$. Many frames show a pattern of 10 bright and weak 'beamlets', and to the extent that a given 'beamlet' configuration remains relatively stable for several frames – thus several circulation times – the $\hat{P}_3$ value used to construct the 'movie' is confirmed.

6 SUMMARY AND DISCUSSION

In the foregoing sections we have conducted a full analysis of the PS modulation of pulsar B1737+13. This relatively bright pulsar attracted our attention because of its relatively rare five-component profile, which gives the opportunity to study a double-cone emission system as well as the central core component. We then find the following.

(i) Its profile consists of five distinct components over a broadband, indicating core/double-cone emission.

(ii) The core lags the mid-point of both conal pairs at 327 and 1400 MHz, and reasonable emission heights are obtained when the shifts are interpreted as reflecting A/R.

(iii) The PSs show intervals with strong and weak component I emission, but have unclear boundaries so cannot be interpreted as modes as did RWS.

(iv) Only around 0.04 per cent of 'null' pulses occur, and these few are probably pseudo-nulls.

(v) At 1.4 GHz a periodicity of roughly $92P_1$ modulates component I strongly and the others more weakly.

(vi) Components I, II and IV are correlated with themselves at delays of $9P_1$ and its multiples, and the strength of the $92P_1$ feature at 1.4 GHz suggests a subbeam carousel of with 10 'beamlets'.

(vii) 'Beamlets' in the outer and inner conal rings appear to rotate with the same period.

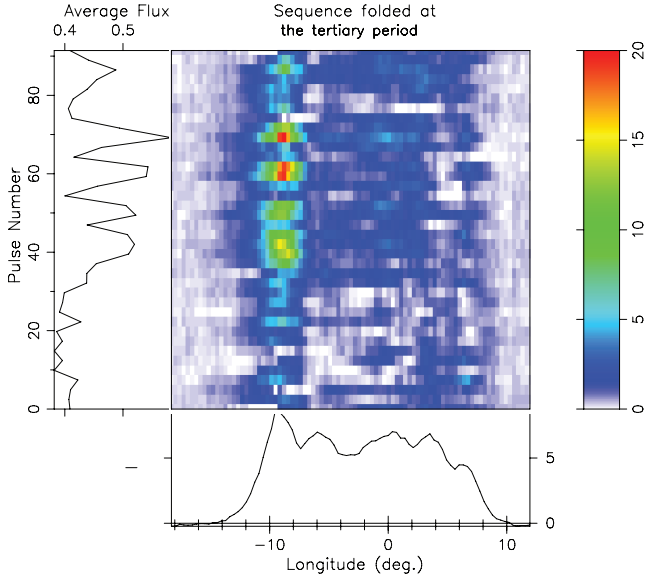

Figure 7. Partial 1400-MHz PS (pulses 1001–2055) folded at $91P_1$ (see Section 5.2) or 10 times the dominant P_3 feature's period of $9.1 \pm 0.1P_1$. The unmodulated 'base', shown in the bottom panel, has been subtracted from the power in the main panel. The weakish component I here is indicative of the star's 'abnormal' behaviour. The four bright features have a spacing that is compatible with a 10-'beamlet' carousel configuration. By folding at 10 times the putative P_3, we are able to observe a regular pattern of bright responses. The rough persistence of a half-illuminated carousel over this (and other) intervals of our observations goes far towards explaining why the low-frequency feature is so prominent in B1737+13.

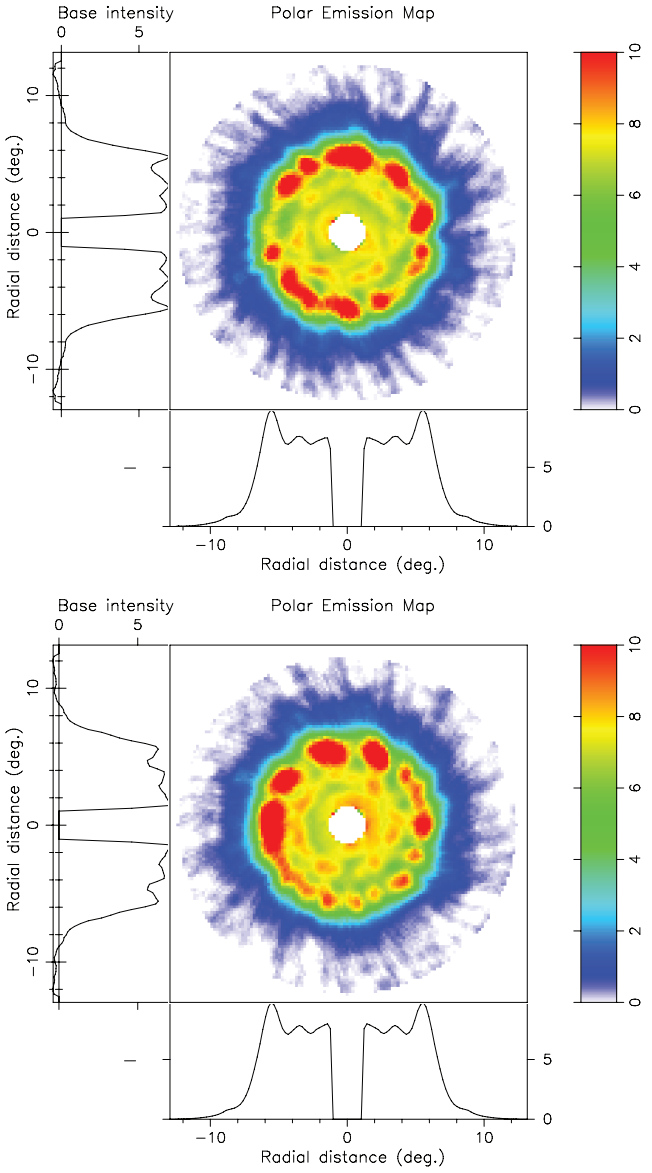

Figure 8. B1737+13 subbeam-carousel 'map' pair at 1400 MHz, using a $\hat{P}_3$ identical to the $10 \times 9.1P_1$ folding period of Fig. 7. The maps display the respective halves of the 2055-pulse observation. The roughly 10-P_3 average maps show a somewhat disordered 'beamlet' configuration (top) and one having four dominant 'beamlets' with a 10-'beamlet' pattern (bottom). Note that both configurations are irregular enough to generate a low-frequency $\hat{P}_3$ fluctuation feature. The 'nearer' rotational pole is at the top of the diagrams; and the magnetic axis is in the centre of the main panels, such that the sightline traverse passes within $1\overset{\circ}{.}9$ ($= \beta$) of this point along the meridian. These maps are somewhat 'overexposed' – that is, saturating in red – so as to show the inner cone structure.

Like other core/double-cone objects, B1737+13 has a nearly central sightline traverse. Like B1237+25, its component I displays stronger and more definable properties than its component V, though the opposite may be true for B0329+54 and B1857−26. B0329+54 and B1237+25 have distinct modes; whereas no clear moding has been identified in either B1737+13 or B1857−26.

Both B0329+54 and B1237+25 exhibit highly active core components, the first participating strongly in its modes and the latter exhibiting A/R. By contrast, the core components of B1737+17 and B1857−26 are relatively steady. In all the four exemplars the core component shows a steeper spectrum than the conal components, and for all but B1737+13 the cone is strongly labelled by antisymmetric circular polarization.

B1237+25 and B1857−26 exhibit 'nulls' of short duration, about 6 and 20 per cent, respectively, and probably these are also pseudo-nulls but this has not been shown conclusively. The null fractions of both B0329+54 and B1737+13 are tiny by contrast.

The analytical results above have shed further light on a pulsar with an unusual five-component profile. Overall, we have been able to show that both its profile and modulation characteristics are fully compatible with the model of a core and double-conical beam. Moreover, its pulse modulation seems to reflect a subbeam carousel with around 10 'beamlets' and a circulation time $\hat{P}_3$ of roughly 92 rotation periods. However, this circulation period is greatly longer than the $1.7P_1$ ($= B_{12}/P^2{}_1$, where B_{12} is the surface magnetic field in units of 10^{12} G) predicted by the Ruderman & Sutherland (1975) model. Indeed, every pulsar with a well-measured $\hat{P}_3$ value shows just this behaviour, apparently indicating that the surface field is screened (Gil et al. 2003, 2008) and/or operates over a larger height range (Harding, Muslimov & Zhang 2002) than this model envisioned.

ACKNOWLEDGMENTS

We are pleased to acknowledge Maciej Serylak and Geoffrey Wright for their critical readings of the manuscript and Jeffrey Herfindal for assistance with aspects of the analysis. We also wish to thank Joel Weisberg for his assistance with the ionospheric Faraday rotation corrections. One of us (JMR) thanks the Anton Pannekoek Astronomical Institute of the University of Amsterdam for their generous hospitality and both Netherlands National Science Foundation and ASTRON for their Visitor Grants. Portions of this work were

carried out with support from US National Science Foundation Grants AST 99-87654 and 08-07691. Arecibo Observatory is operated by Cornell University under contract to the US NSF. This work used the NASA ADS system.

REFERENCES

Backer D. C., 1970, Nat, 228, 42
Deich W. T. S., 1986, Thesis, Cornell Univ., Ithaca, NY
Deshpande A. A., Rankin J. M., 2001, MNRAS, 322, 438 (DR01)
Dyks J., Rudak B., Harding A. K., 2004, ApJ, 607, 939
Edwards R. T., Stappers B. W., 2004, A&A, 421, 681
Gangadhara R. T., Gupta Y., 2001, ApJ, 555, 31 (G&G)
Gil J., Melikidze G. I., Geppert U., 2003, A&A, 407, 315
Gil J., Haberl F., Melkidze G., Zhang B., Melkidze G., Jr, 2008, ApJ, 686, 497
Gould D. M., Lyne A. G., 1998, MNRAS, 301, 253
Hankins T. H., Rankin J. M., 2010, AJ, 139, 168
Hankins T. H., Rickett B. J., 1986, ApJ, 311, 684
Harding A. K., Muslimov A. G., Zhang B., 2002, ApJ, 576, 366
Herfindal J. L., Rankin J. M., 2007, MNRAS, 380, 430
Herfindal J. L., Rankin J. M., 2009, MNRAS, 393, 1391 (HR0709)
Hobbs G., Lorimer D. R., Lyne A. G., Kramer M., 2005, MNRAS, 360, 974
Johnston S., Hobbs G., Vigeland S., Kramer M., Weisberg J. M., Lyne A. G., 2006, MNRAS, 364, 1397
Lyne A. G., Manchester R. N., 1988, MNRAS, 234, 477
Maan Y., Deshpande A. A., 2008, in Bassa C. G., Wang Z., Cumming A., Kaspi V. M., eds, AIP Conf. Proc. Vol. 983, 40 Years of Pulsars: Millisecond Pulsars, Magnetars and More. Am. Inst. Phys., New York, p. 103
Malov I. F., Suleymanova S. A., 1998, Astron. Rep., 42, 388
Mitra D., Rankin J. M., 2002, ApJ, 577, 322
Mitra D., Rankin J. M., 2008, MNRAS, 385, 606
Mitra D., Rankin J., Gupta Y., 2007, MNRAS, 379, 932
Rankin J. M., 1993a, ApJ, 405, 285 (ET VI)
Rankin J. M., 1993b, ApJS, 85, 145 (ET VI)
Rankin J. M., 2007, ApJ, 664, 443
Rankin J. M., Wright G. A. E., 2007, MNRAS, 379, 507
Rankin J. M., Wright G. A. E., 2008, MNRAS, 385, 606
Rankin J. M., Wolszczan A., Stinebring D. R., 1988, ApJ, 324, 1048 (RWS)
Rankin J. M., Stinebring D. R., Weisberg J. M., 1989, ApJS, 324, 1048
Ruderman M. A., Sutherland P. G., 1975, ApJ, 197, 51
Srostlik Z., Rankin J. M., 2005, MNRAS, 362, 1121 (SR05)
Wang N., Manchester R. N., Johnston S., 2007, MNRAS, 377, 1383
Weltevrede P., Edwards R. T., Stappers B. W., 2006, A&A, 445, 243
Weltevrede P., Stappers B. W., Edwards R. T., 2007, A&A, 469, 607

APPENDIX A

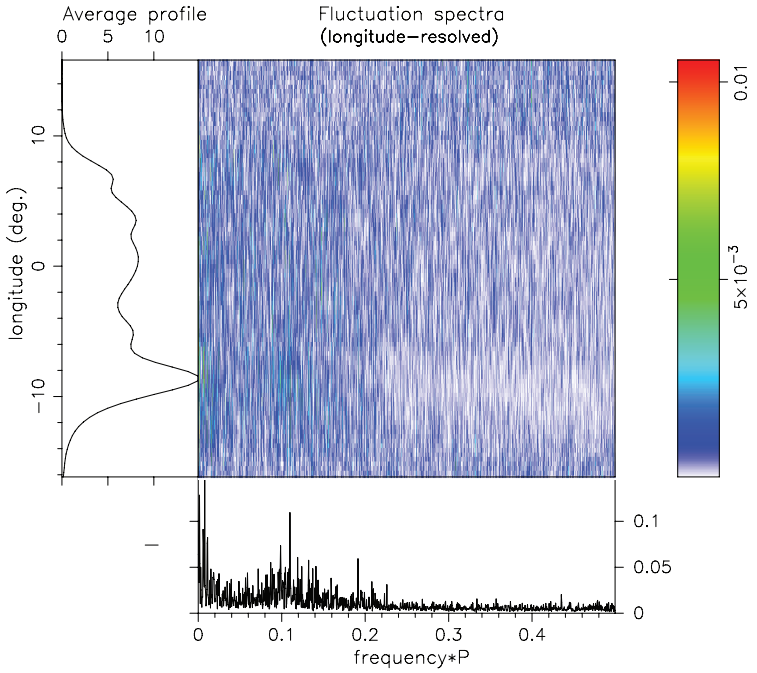

Figure A1. Longitude-resolved fluctuation spectra for the entire B1737+13 PS at 1400 MHz as in Fig. 3, employing an FFT length of 2048. The primary low-frequency and 'drift'-modulation features have component-weighted periods of 91 ± 2 and $9.1 \pm 0.1P_1$, respectively.

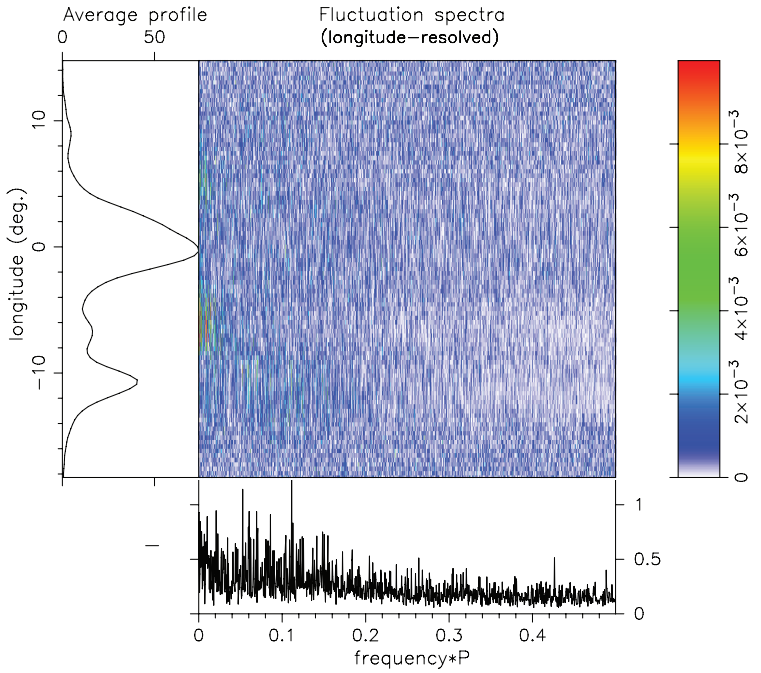

Figure A2. Longitude-resolved fluctuation spectra as in Fig. A1 for the entire B1737+13 PS at 327 MHz, employing an FFT length of 2048. The brightest feature corresponds to amplitude-modulated power in component I with a periodicity of $8.98 \pm 0.10 P_1$. No low-frequency response is prominent in the integral spectrum. Closer study shows that the 9-P_1 feature is stable only over the middle of the PS, between roughly pulses 400 and 2000.

This paper has been typeset from a TEX/LATEX file prepared by the author.